Inorganic Chemistry
Article

Inorg. Chem. **2009**, *48*, 5263–5268 **5263**
DOI: 10.1021/ic900217t

Porous Metal-Organic Frameworks Based on an Anthracene Derivative: Syntheses, Structure Analysis, and Hydrogen Sorption Studies

Shengqian Ma,*,‡ Jason M. Simmons,§,∥ Daofeng Sun,† Daqiang Yuan,† and Hong-Cai Zhou*,†

†*Department of Chemistry, Texas A&M University, P.O. Box 30012, College Station, Texas 77842,* ‡*Chemical Sciences and Engineering Division, Argonne National Laboratory, 9700 S. Cass Avenue, Argonne, Illinois 60439,* §*NIST Center for Neutron Research, National Institute of Standards and Technology, Gaithersburg, Maryland 20899 and* ∥*Department of Materials Science and Engineering, University of Pennsylvania, Philadelphia, Pennsylvania 19104*

Received February 3, 2009

Solvothermal assembly of 5,5′-(9,10-anthracenediyl)di-isophthalate (H_4adip) with in situ-generated dicopper and diiron paddlewheel secondary building units (SBUs) afforded two porous metal-organic frameworks (MOFs), designated as PCN-14 and PCN-15, respectively. The two MOFs crystallize in different structures, characterized by a difference in the dihedral angles between the anthracene and the phenyl rings of the adip ligand. PCN-14 retains permanent porosity under dehydration and contains nanoscopic cages while PCN-15 contains only one-dimensional hexagonal channels along the (0 0 1) direction which require solvent stabilization. The aromaticity of the anthracene rings of the adip ligand in conjunction with the nanoscopic cages grants PCN-14 high excess hydrogen adsorption capacity of 2.70 wt % at 77 K, 760 Torr (4.42 wt % at saturation), as well as high hydrogen affinity of 8.6 kJ/mol at low H_2 coverage. These values are compared to other tetracarboxylate-derived MOFs to better understand the role of the aromatic rings in hydrogen adsorption.

Introduction

Increasing research interest has recently been drawn to the exploration of porous metal-organic frameworks (MOFs)[1−17] as promising candidates to approach the U.S. DOE targets for on-board hydrogen storage applications.[18] Compared to other porous materials such as activated carbon, nanotubes, and zeolites,[19−23] porous MOFs possess the advantages of well-defined specific hydrogen binding sites[24−28] together with functionalizable pore walls[29] capable of increasing hydrogen interaction energies.

Recent inelastic neutron scattering (INS)[27] and neutron powder diffraction (NPD)[25,26] studies of porous MOFs

*To whom correspondence should be addressed. E-mail: sma@anl.gov (S.M.), zhou@mail.chem.tamu.edu (H.-C.Z.).

(1) Ma, S.; Sun, D.; Ambrogio, M. W.; Fillinger, J. A.; Parkin, S.; Zhou, H.-C. *J. Am. Chem. Soc.* **2007**, *129*, 1858–1859.
(2) Zhao, D.; Yuan, D.; Zhou, H.-C. *Energy Environ. Sci.* **2008**, *1*, 222–235.
(3) Dincă, M.; Long, J. R. *Angew. Chem., Int. Ed.* **2008**, *47*, 6766–6779.
(4) Furukawa, H.; Miller, M. A.; Yaghi, O. M. *J. Mater. Chem.* **2007**, *17*, 3197–3204.
(5) Collins, D. J.; Zhou, H.-C. *J. Mater. Chem.* **2007**, *17*, 3154–3160.
(6) Wong-Foy, A. G.; Matzger, A. J.; Yaghi, O. M. *J. Am. Chem. Soc.* **2006**, *128*, 3494–3495.
(7) Sun, D.; Ma, S.; Ke, Y.; Collins, D. J.; Zhou, H.-C. *J. Am. Chem. Soc.* **2006**, *128*, 3896–3897.
(8) Ma, S.; Eckert, J.; Forster, P. M.; Yoon, J.; Hwang, Y. K.; Chang, J.-S.; Collier, C. D.; Parise, J. B.; Zhou, H.-C. *J. Am. Chem. Soc.* **2008**, *130*, 15896–15902.
(9) Ma, S.; Zhou, H.-C. *J. Am. Chem. Soc.* **2006**, *128*, 11734–11735.
(10) Lin, X.; Jia, J.; Zhao, X.; Thomas, K. M.; Blake, A. J.; Walker, G. S.; Champness, N. R.; Hubberstey, P.; Schröder, M. *Angew. Chem., Int. Ed.* **2006**, *45*, 7358–7364.
(11) Latroche, M.; Surblé, S.; Serre, C.; Mellot-Draznieks, C.; Llewellyn, P. L.; Lee, J.-H.; Chang, J.-S.; Jhung, S. H.; Férey, G. *Angew. Chem., Int. Ed.* **2006**, *45*, 8227–8231.
(12) Forster, P. M.; Eckert, J.; Heiken, B. D.; Parise, J. B.; Yoon, J. W.; Jhung, S. H.; Chang, J. S.; Cheetham, A. K. *J. Am. Chem. Soc.* **2006**, *128*, 16846–16850.
(13) Dincă, M.; Dailly, A.; Liu, Y.; Brown, C. M.; Neumann, D. A.; Long, J. R. *J. Am. Chem. Soc.* **2006**, *128*, 16876–16883.
(14) Chen, B.; Ma, S.; Zapata, F.; Lobkovsky, E. B.; Yang, J. *Inorg. Chem.* **2006**, *45*, 5718–5720.
(15) Kesanli, B.; Cui, Y.; Smith, M. R.; Bittner, E. W.; Bockrath, B. C.; Lin, W. *Angew. Chem., Int. Ed.* **2005**, *44*, 72–75.
(16) Ma, S.; Sun, D.; Wang, X.-S.; Zhou, H.-C. *Angew. Chem., Int. Ed.* **2007**, *46*, 2458–2462.
(17) (a) Ma, S.; Wang, X.-S.; Yuan, D.; Zhou, H.-C. *Angew. Chem., Int. Ed.* **2008**, *47*, 4130–4133. (b) Ma, S.; Yuan, D.; Wang, X.-S.; Zhou, H.-C. *Inorg. Chem.* **2009**, *48*, 2072–2077. (c) Papaefstathiou, G. S.; MacGillivray, L. R. *Angew. Chem., Int. Ed.* **2002**, *41*, 2070–2073.
(18) *DOE Office of Energy Efficiency and Renewable Energy Hydrogen, Fuel Cells & Infrastructure Technologies Program Multi-Year Research, Development and Demonstration Plan*, available at http://www.eere.energy.gov/hydrogenandfuelcells/mypp.
(19) Züttel, A.; Wenger, P.; Sudan, P.; Mauron, P.; Orimo, S.-i. *Mater. Sci. Eng., B* **2004**, *108*, 9–18.
(20) Jung, J. H.; Han, W. S.; Rim, J. A.; Lee, S. J.; Cho, S. J.; Kim, S. Y.; Kang, J. K.; Shinkai, S. *Chem. Lett.* **2006**, *35*, 32–33.
(21) Weck, P. F.; Kim, E.; Balakrishnan, N.; Cheng, H.; Yakobson, B. I. *Chem. Phys. Lett.* **2007**, *439*, 354–359.
(22) Thomas, K. M. *Catal. Today* **2007**, *120*, 389–398.
(23) Lachance, P.; Bénard, P. *Int. J. Green Energy* **2007**, *4*, 377–384.

Published on Web 04/23/2009

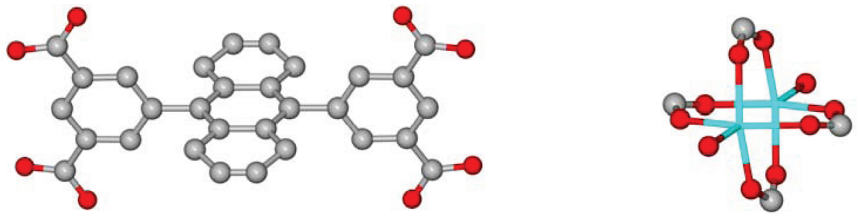

(a) (b)

Figure 1. (a) H_4adip ligand; (b) $M_2(COO)_4(H_2O)_2$ (M = Cu, Fe) paddlewheel SBU. Color sheme: C, gray; O, red; M, turquoise.

revealed the inorganic metal clusters as the initial hydrogen binding sites with successive adsorption sites located over the phenyl rings of the organic linkers. Although the primary hydrogen binding sites are metal-based, the functionalization of organic linkers plays an important role in further enhancing hydrogen adsorption capacities of porous MOFs.[30] Computational studies by Sagara et al. suggested that it is possible to bind two H_2 molecules on each side of the 2, 6-naphthalenedicarboxylate linker in IRMOF-8, and proposed that additional aromatic rings in the frameworks could potentially serve as hydrogen adsorption sites.[31] Increasing the aromaticity of the organic linkers has been both theoretically predicted[31,32] and experimentally proven[30,33] to be an effective way to improve hydrogen adsorption capacities of porous MOFs.

Taking the above into consideration, we designed a ligand, 5,5′-(9,10-anthracenediyl)di-isophthalate (H_4adip) (Figure 1a) and expect the central anthracene to provide additional hydrogen binding sites thus increasing the hydrogen uptake. Under solvothermal conditions, reactions of H_4adip with $Cu(NO_3)_2$ and $FeCl_2$ gave rise to two porous MOFs designated as PCN-14 and PCN-15 respectively (PCN represents porous coordination network). In this contribution, we report the synthesis and detailed structural description of PCN-15, along with a comparison of the structural properties and hydrogen storage performances of both PCN-14 and PCN-15.

Experimental Section

Synthesis of PCN-14 and PCN-15. PCN-14 was prepared according to the procedures described in our previous work.[34] PCN-15 was synthesized by heating a sealed Pyrex tube with a mixture of H_4adip ligand (0.005 g, 1.4×10^{-5} mol) and $FeCl_2$ (0.02 g, 1.6×10^{-5} mol) in 1.5 mL DMSO (dimethyl sulfoxide) together with 6 drops dimethylformamide (DMF) and 3 drops HBF_4 (40% aqua) at 120 °C for 3 days followed by cooling to room temperature at a rate of 0.1 °C/min. The DMF was added to preclude the complete oxidation of iron to Fe^{3+} to ensure the formation of the proper SBU. The resulting orange block crystals were washed with DMSO in a glovebox under nitrogen atmosphere (yield: 75% based on the adip ligand), and have a formula of $Fe_6(H_2O)_6(adip)_3Cl\cdot 9DMSO\cdot 12H_2O$, which was derived from crystallographic data and elemental analysis (calcd: C, 44.64; H, 4.58; Cl, 4.13. Found: C, 44.55; H, 4.62; Cl, 4.21).

Table 1. Crystal Data[a] and Structure Refinement of PCN-14, PCN-15

	PCN-14	PCN-15
formula	$C_{270}H_{162}Cu_{18}O_{90}$	$C_{90}H_{54}ClFe_6O_{30}$
FW	5989.9	1985.88
crystal system	rhombohedral	rhombohedral
space group	$R\bar{3}c$	$R\bar{3}m$
a, Å	18.4530(4)	27.1117(9)
b, Å	18.4530(4)	27.1117(9)
c, Å	76.976(4)	16.5413(1)
α, deg	90.00	90.00
β, deg	90.00	90.00
γ, deg	120.00	120.00
V, Å^3	22699.7 (1)	10529.6 (1)
Z	2	3
d_{calc} g cm^{-1}	0.871	0.940
R_1, wR_2[b]	0.0518, 0.1591	0.1088, 0.3462

[a] Obtained with graphite-monochromated Mo Kα (λ = 0.71073 Å) radiation. [b] $R_1 = \sum||F_o| - |F_c||/\sum|F_o|$ and $wR_2 = \{\sum w(F_o^2 - F_c^2)^2/\sum w(F_o^2)^2\}^{1/2}$.

Single-Crystal X-ray Crystallography. Single crystal X-ray data of PCN-15 were collected on a Bruker Smart Apex diffractometer[35] equipped with an Oxford Cryostream low temperature device and a fine-focus sealed-tube X-ray source (Mo Kα radiation, λ = 0.71073 Å, graphite monochromated) operating at 45 kV and 35 mA. Frames were collected with 0.3° intervals in φ and ω for 60 s per frame such that a hemisphere of data was collected. Raw data collection and refinement were done using SMART. Data reduction was performed using SAINT+ and corrected for Lorentz and polarization effects.[36] The structure was solved by direct methods and refined by full-matrix least-squares on F^2 with anisotropic displacement using SHELX-97.[37] Non-hydrogen atoms were refined with anisotropic displacement parameters during the final cycles. Hydrogen atoms on carbon

(24) Spencer, E. C.; Howard, J. A. K.; McIntyre, G. J.; Rowsell, J. L. C.; Yaghi, O. M. *Chem. Commun.* **2006**, 278–280.
(25) Peterson, V. K.; Liu, Y.; Brown, C. M.; Kepert, C. J. *J. Am. Chem. Soc.* **2006**, *128*, 15578–15579.
(26) Yildirim, T.; Hartman, M. R. *Phys. Rev. Lett.* **2005**, *95*, 215504.
(27) Rowsell, J. L. C.; Eckert, J.; Yaghi, O. M. *J. Am. Chem. Soc.* **2005**, *127*, 14904–14910.
(28) Chen, B.; Zhao, X.; Putkham, A.; Hong, K.; Lobkovsky, E. B.; Hurtado, E. J.; Fletcher, A. J.; Thomas, K. M. *J. Am. Chem. Soc.* **2008**, *130*, 6411–6423.
(29) Eddaoudi, M.; Kim, J.; Rosi, N.; Vodak, D.; Wachter, J.; O'Keeffe, M.; Yaghi, O. M. *Science* **2002**, *295*, 469–472.
(30) Rowsell, J. L. C.; Yaghi, O. M. *J. Am. Chem. Soc.* **2006**, *128*, 1304–1315.
(31) Sagara, T.; Klassen, J.; Ortony, J.; Ganz, E. *J. Chem. Phys.* **2005**, *123*, 014701–014704.
(32) Han, S. S.; Deng, W.-Q.; Goddard, W. A. *Angew. Chem., Int. Ed.* **2007**, *46*, 6289–6292.
(33) Rowsell, J. L. C.; Millward, A. R.; Park, K. S.; Yaghi, O. M. *J. Am. Chem. Soc.* **2004**, *126*, 5666–5667.
(34) Ma, S.; Sun, D.; Simmons, J. M.; Collier, C. D.; Yuan, D.; Zhou, H.-C. *J. Am. Chem. Soc.* **2008**, *130*, 1012–1016.
(35) Note: Certain commercial suppliers are identified in this paper to foster understanding. Such identification does not imply recommendation or endorsement by the National Institute of Standards and Technology, nor does it imply that the materials or equipment identified are necessarily the best available for the purpose.
(36) *SAINT+*, version 6.22; Bruker Analytical X-Ray Systems, Inc.: Madison, WI, 2001.
(37) Sheldrick, G. M. *SHELX-97*; Bruker Analytical X-Ray Systems, Inc.: Madison, WI, 1997.

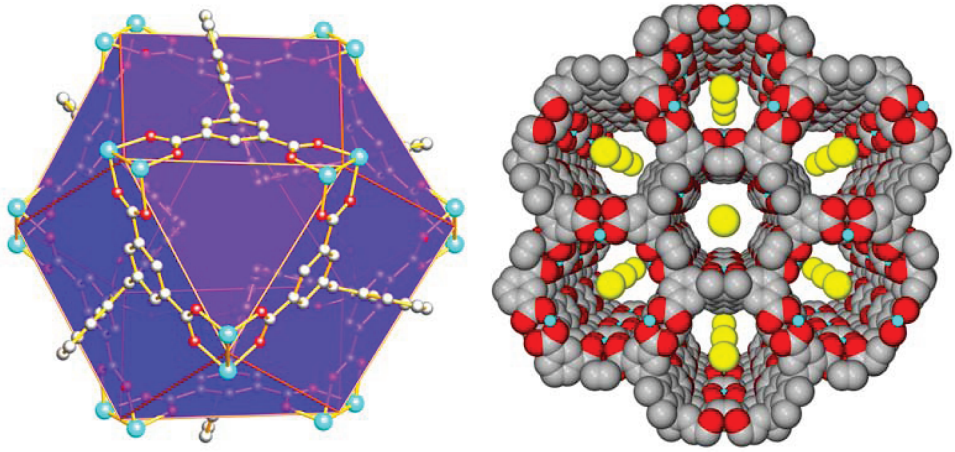

Figure 2. (a) Nanoscopic cage in PCN-14; (b) one-dimensional hexagonal channels of PCN-15 occupied by chlorine anions viewed along the (0 0 1) direction.

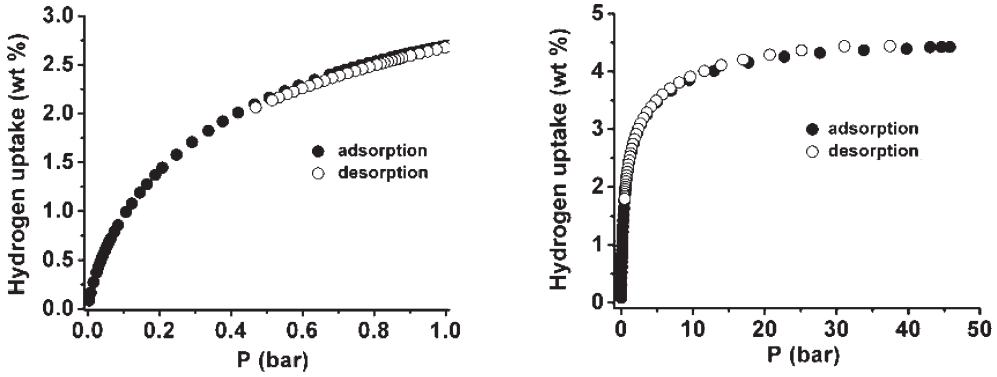

Figure 3. (a) Low-pressure H_2 sorption isotherms of PCN-14 at 77 K; (b) High-pressure excess H_2 sorption isotherms of PCN-14 at 77 K.

were calculated in ideal positions with isotropic displacement parameters set to 1.2 × U_{eq} of the attached atom. Absorption corrections were applied using SADABS after the formula of the compound was determined approximately.[36] Solvent molecules in the structure were highly disordered and were impossible to refine using conventional discrete-atom models. To resolve these issues, the contribution of solvent electron density was removed by the SQUEEZE routine in PLATON.[38] CCDC-682384 (PCN-15) contains the supplementary crystallographic data, which can be obtained free of charge at www.ccdc.cam.ac.uk/conts/retrieving.html (or from the Cambridge Crystallographic Data Center, 12, Union Road, Cambridge CB21EZ, U.K.; fax: (+44) 1223−336−033; or deposit@ccdc.cam.ac.uk).

Gas Sorption Measurements. The low-pressure adsorption measurements were performed at 77 K and 0−760 torr on a Beckman Coulter SA 3100 surface area and pore size analyzer. An as-isolated sample of PCN-14 was immersed in methanol for 24 h, and the extract was decanted. Fresh methanol was subsequently added, and the crystals were allowed to stay for an additional 24 h to remove the nonvolatile solvates (DMF and H_2O). The sample was collected by decanting and treated with dichloromethane similarly to removing methanol solvates. For PCN-15, similar procedures were handled in the glovebox full of N_2 atmosphere but with only THF as exchanging solvent. After the removal of dichloromethane by decanting, the sample was dried under a dynamic vacuum ($< 10^{-3}$ torr) at room temperature (25 °C) overnight. Before the measurement, the sample was dried again by using the "outgas" function of the surface area analyzer for 4 h at 120 °C. Sorption measurements were performed using high purity nitrogen (99.999%) and hydrogen (99.9995%) on a sample of 100 mg with the temperature maintained at 77 K by liquid nitrogen. For the hydrogen adsorption measurement, the regulator and pipe were flushed with hydrogen before connecting to the analyzer. The internal lines of the instrument were flushed three times by utilizing the "flushing lines" function of the program to ensure the purity of H_2. High pressure hydrogen sorption isotherm measurements on PCN-14 were performed using a home-built fully computer-controlled Sievert apparatus using scientific grade hydrogen (99.9999% purity). The detailed specifications of the Sievert apparatus and the data analysis can be found elsewhere.[39] Prior to measurement, about 200 mg solvent-exchanged sample was activated under vacuum (less than 10^{-4} torr) by first heating at room temperature overnight, and then at 120 °C for at least 4 h. Once activated, the samples were loaded into the measurement cell inside a He-glovebox to prevent rehydration/deactivation.

Results and Discussion

Crystal Structure Description. Single crystal X-ray analysis revealed that both PCN-14 and PCN-15 adopt the $M_2(COO)_4(H_2O)_2$ (M = Cu, Fe) paddlewheel as their secondary building units (SBUs) (Figure 1b), but with PCN-14 crystallizing in space group $R\bar{3}c$ while PCN-15 crystallizes in space group $R\bar{3}m$ (Table 1). The Cu−Cu distance is 2.654 Å, and the Cu−aqua distance is 2.122 Å for the paddlewheel SBU found in PCN-14, while the distance of Fe−Fe is 3.094 Å and that of the Fe−aqua is

(38) Spek, A. L. *J. Appl. Crystallogr.* **2003**, *36*, 7–13.

(39) Zhou, W.; Wu, H.; Hartman, M. R.; Yildirim, T. *J. Phys. Chem. C.* **2007**, *111*, 16131.

Scheme 1. Tetracarboxylate Ligands Employed for the Construction of NbO Type MOFs[a]

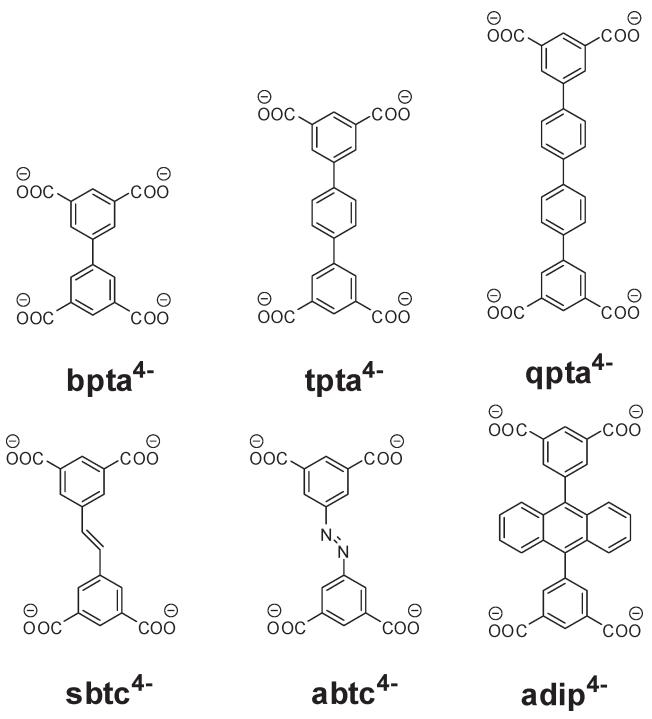

[a] bpta = biphenyl-3,3′,5,5′-tetracarboxylate; tpta = terphenyl-3,3′,5,5′-tetracarboxylate; qpta = quaterphenyl-3,3′,5,5′-tetracarboxylate; sbtc = *trans*-stilbene-3,3′,5,5′-tetracarboxylate; abtc = azobenzene-3,3′,5,5′-tetracarboxylate; adip = 5,5′-(9,10-anthracenediyl)di-isophthalate.

2.288 Å for the paddlewheel SBU in PCN-15. The distances of Cu and oxygen of the carboxylate groups of the adip ligand range from 1.940 Å to 1.960 Å in PCN-14, while those of Fe and oxygen of the carboxylate groups of the adip ligand range from 2.049 Å to 2.059 Å in PCN-15.

The structure of PCN-14 was described in our previous work,[34] and consists of nanoscopic cages, each with a volume of 1150 $Å^3$ (Figure 2a). In contrast, PCN-15 contains no cages, having only one-dimensional hexagonal channels along the (0 0 1) direction with a size of 13.636 Å (atom to atom distance) (Figure 2b). Chlorine anions (yellow sphere in Figure 2b) reside at the center of the hexagonal channels indicating a mixture of +2 and +3 oxidation states for Fe in PCN-15. Calculated using PLATON/SOLV,[38] the solvent accessible volume of PCN-14 is 63.5% and that of PCN-15 is 47.9%.

Although PCN-14 and PCN-15 are constructed from the same ligand and the same SBU, their structures are quite different and crystallize in different space groups. Even though the cause is not fully understood and may be due to subtle differences in the synthesis conditions, the resulting structures possess different dihedral angles between the anthracene and the phenyl rings of the adip ligand in PCN-14 and PCN-15. In PCN-14, the dihedral angle is 70.4° (Supporting Information, Figure S2a), leading to reduced repulsion from adjacent anthracene rings. This angle supports the formation of cages, as well as lowers the crystal symmetry to $R\bar{3}c$. This symmetry is different from previously reported MOFs based on tetracarboxylate ligands and dicopper paddlewheel SBUs, all of which crystallize in $R\bar{3}m$.[10,40,41] In contrast, the dihedral angle in PCN-15 is near 90° (87.0°) (Supporting Information, Figure S2b). This renders the adip ligand with mirror plane symmetry and leads to the $R\bar{3}m$ crystal symmetry which is the same as the previously reported MOFs with NbO type structure. The near 90° dihedral angle between the anthracene and the phenyl rings of the adip ligand results in large repulsions between the anthracene rings of adjacent adip ligands thus inhibiting the formation of cages and forcing the formation of only one-dimensional channels in PCN-15.

The permanent porosities of PCN-14 and PCN-15 were checked by N_2 sorption measurements at 77 K. N_2 sorption isotherms (Supporting Information, Figure S2) of a newly prepared batch of PCN-14 sample, which was fully activated according to the procedure described before,[34] confirmed its sorption reversibility and gave an estimated Brunauer−Emmett−Teller (BET) surface area of 1753 m^2/g which is consistent with the previously reported result. In contrast, a sample of PCN-15 was activated by solvent-exchanging the freshly prepared sample with THF in a glovebox followed by evacuation under dynamic vacuum at 50 °C overnight. N_2 sorption isotherms of activated PCN-15 sample revealed that it adsorbed little N_2 (Supporting Information, Figure S3) and has negligible surface area.

Hydrogen Sorption Studies. The high porosity and nanoscopic cages in PCN-14 prompted us to evaluate its hydrogen adsorption performance. Low-pressure hydrogen sorption isotherms of the fully activated PCN-14 sample at 77 K revealed reversible hydrogen adsorption as shown Figure 3. At 77 K and 760 Torr, the excess gravimetric hydrogen uptake capacity of PCN-14 can reach 2.70 wt %, which is among the highest of reported MOFs under similar conditions.[10,30,40−42] The hydrogen uptake values of low-pressure hydrogen sorption isotherms are also consistent with those of high-pressure sorption isotherms within comparable pressure region. At higher pressure, the excess gravimetric hydrogen uptake of PCN-14 reaches saturation with a value of 4.42 wt %. This corresponds to a volumetric uptake of 36.6 g/L calculated using the crystal density of dehydrated PCN-14 (0.829 g/cm^3). In contrast, low pressure H_2 isotherms in PCN-15 show limited H_2 uptake (< 40 cm^3/g) after activation at 50 °C or even 150 °C (Supporting Information, Figure S4). The low uptake of N_2 and H_2 in PCN-15 indicates that it does not retain significant permanent porosity and may require the solvent to stabilize the structure.

To understand how ligand functionalization affects the hydrogen uptake capacity, it is useful to compare the performance of PCN-14 with that of other reported NbO-type porous MOFs that are constructed from dicopper paddlewheel SBUs and tetracarboxylate ligands (Scheme 1). For hydrogen adsorption at 77 K, 760 Torr,

(40) Chen, B.; Ockwig, N. W.; Millward, A. R.; Contreras, D. S.; Yaghi, O. M. *Angew. Chem., Int. Ed.* **2005**, *44*, 4745–4749.

(41) Wang, X.-S.; Ma, S.; Rauch, K.; Simmons, J. M.; Yuan, D.; Wang, X.; Yildirim, T.; Cole, W. C.; López, J. J.; Meijere, A. De; Zhou, H.-C. *Chem. Mater.* **2008**, *20*, 3145–3152.

(42) Wang, X.-S.; Ma, S.; Forster, P. M.; Yuan, D.; Eckert, J.; Lopez, J. J.; Murphy, B. J.; Parise, J. B.; Zhou, H.-C. *Angew. Chem., Int. Ed.* **2008**, *47*, 7263–7266.

Table 2. Physical Characteristics and Hydrogen Adsorption Properties of NbO Typed Porous MOFs Based on Tetracarboxylate Ligands and Dicopper Paddlewheel SBU

	BET surface area (m^2/g)	solvent accessible volume[a] (%)	calculated crystal density (g/cm^3)	H_2 uptake at 77 K, 760 Torr (wt %)	gravimetric H_2 saturation uptake at 77 K (wt %)	volumetric H_2 saturation uptake at 77 K (g/L)
PCN-14 (adip)	1753	63.5	0.829	2.70	4.42	36.6[b]
MOF-505 (bpta)[10]	1670	63.3	0.927	2.59	4.20	38.9
Cu-tpta[10]	2247	70.4	0.886	2.52	6.70	43.6
Cu-qpta[10]	2932	75.5	0.587	2.24	7.01	41.1
PCN-10 (abtc)[41]	1407	71.2	0.825	2.34	4.20	34.7[b]
PCN-11 (sbtc)[41]	1779	71.9	0.805	2.55	5.04	40.6[b]

[a] Calculated using PLATON/SOLV.[35] [b] Calculated from multiplying the gravimetric uptake by ideal dehydrated crystal density.

it can be seen from Table 2 that increasing the size of the cages by elongating the bpta ligand with one or two phenyl rings leads to a steady decrease of hydrogen uptake in Cu-tpta and Cu-qpta.[10] Assuming that the hydrogen binds first to the open Cu-sites, as seen in other Cu paddlewheel MOFs,[25,28] this decrease can be attributed to reduced potential well overlaps near the Cu-site resulting from the enlarged pore sizes.[30,43] Our previous attempts to enhance hydrogen uptake by grafting double-bond functionalities in PCN-10 and PCN-11 resulted in the same relationship according to size, indicating negligible contribution from unsaturated π-bonds.[41] Stronger binding to the Cu-site, typically accounting for ~1 wt % uptake when fully saturated, could allow for increased filling of the ligand sites at lower pressures, leading to a higher uptake near 1 bar. However, expanding the aromatic conjugation by adding two fused rings greatly favors the low pressure hydrogen adsorption in PCN-14, exhibiting the highest, 1 bar, hydrogen uptake of 2.70 wt % among the six NbO-type porous MOFs. This is also consistent with recent theoretical calculations that an increase in the number of fused rings would boost hydrogen uptake in porous MOFs.[31,32]

Though the extra phenyl rings enhance the initial binding of H_2 to the framework, the saturation hydrogen uptakes scale with surface areas as observed in other types of porous MOFs.[5] The extension of the bpta ligand by adding phenyl rings or double bonds leads to an increase in surface areas with almost proportional increases of hydrogen adsorption capacities at saturation, particularly for Cu-tpta and Cu-qpta. The relatively low surface area of PCN-14 can be ascribed to the bulkiness of the anthracene rings which block partial pores thus resulting in only moderate hydrogen uptake of 4.42 wt % at saturation.

The strength of interactions between the framework and hydrogen can be reflected by isosteric heats of adsorption Q_{st}. The isosteric heat of adsorption of hydrogen in PCN-14 was calculated utilizing the Clausius-Clapeyron equation,[39,44]

$$Q_{st} = -R\,\mathrm{d}(\ln P)/\mathrm{d}(1/T)$$

using isotherms measured at 77, 80, and 87 K (Supporting Information, Figure S5). As shown in Figure 4, the Q_{st} of hydrogen adsorbed in PCN-14 is 8.6 kJ/mol at low

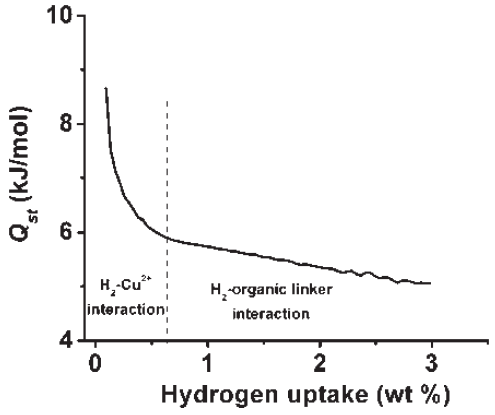

Figure 4. Isosteric heats of adsorption of H_2 in PCN-14.

(0.1 wt %) H_2 loading and decreases to 5.0 kJ/mol at the higher coverage (3.0 wt %). Assuming that the hydrogen binds first to the open Cu^{2+} centers of the paddlewheel SBU as suggested by recent neutron powder diffraction studies of Cu-BTC,[25] the isosteric heat measured up to 0.63 wt %, corresponding to full saturation of the Cu^{2+} sites, can be approximately associated with the Cu^{2+}–H_2 interaction including any increased binding near the Cu-site because of the ligand. This value lies in the range of 8.6 to 5.9 kJ/mol, where the range most likely indicates that secondary sites are also being filled at 77 K before the Cu^{2+} site is fully saturated. The relatively higher initial Q_{st} for H_2 in PCN-14 as compared to other porous MOFs[30,41] based on the dicopper paddlewheel SBU could be attributed to the small pore size[28,45] defined by the anthracene rings if a similar contribution from coordinatively unsaturated copper sites is considered. The Q_{st} value in the range of 5.9−5.0 kJ/mol for H_2 coverage from 0.63 to 3.0 wt % could then correspond largely to H_2–organic linker van der Waals interactions, and is consistent with measurements in other MOFs that rely on purely van der Waals interactions.[39]

Conclusions

In summary, two porous MOFs, PCN-14 and PCN-15, based on an anthracene derivative tetracarboxylate ligand and dimetal paddlewheel SBUs have been constructed and structurally described. Despite being built from the same ligand and the same type of SBUs, PCN-14 consists of nanoscopic cages while PCN-15 contains only one-dimensional channels along the (0 0 1) direction. The structures

(43) Rowsell, J. L. C.; Yaghi, O. M. *Angew. Chem., Int. Ed.* **2005**, *44*, 4670–4679.
(44) Rouquerol, J.; Rouquerol, F.; Sing, K. *Adsorption by Powders and Porous Solids*; Academic Press: London, 1998.
(45) Dinca, M.; Long, J. R. *J. Am. Chem. Soc.* **2005**, *127*, 9376–9377.

differ significantly in their dihedral angles between the anthracene and the phenyl rings of the adip ligands. N_2 sorption analysis revealed that PCN-14 retains its permanent porosity and has a BET surface area of 1753 m^2/g while PCN-15 does not maintain permanent porosity after activation. H_2 sorption studies indicated that the anthracene grants PCN-14 high excess hydrogen uptake capacity of 2.70 wt % at 77 K, 760 Torr but saturation at only 4.42 wt %. Though the ultimate sorption capacity is lower than similar Cu−MOFs because of the smaller effective surface area, the nanoscopic cages permit a more effective potential overlap near the Cu^{2+} site, leading to the relatively higher initial Q_{st} of 8.6 kJ/mol.

Acknowledgment. This work was supported by the Department of Energy (DE-FC36-07GO17033) and the National Science Foundation (CHE-0449634). S.M. acknowledges the Director's Postdoctoral Fellowship from Argonne National Laboratory. J.M.S. also acknowledges support from DOE (BES DE-FG02-98ER45701). The diffractometer was funded by NSF Grant EAR-0003201.

Supporting Information Available: Structure pictures and N_2/H_2 sorption isotherms of PCN-14/15, TGA plot, and PXRD patterns. This material is available free of charge via the Internet at http://pubs.acs.org.